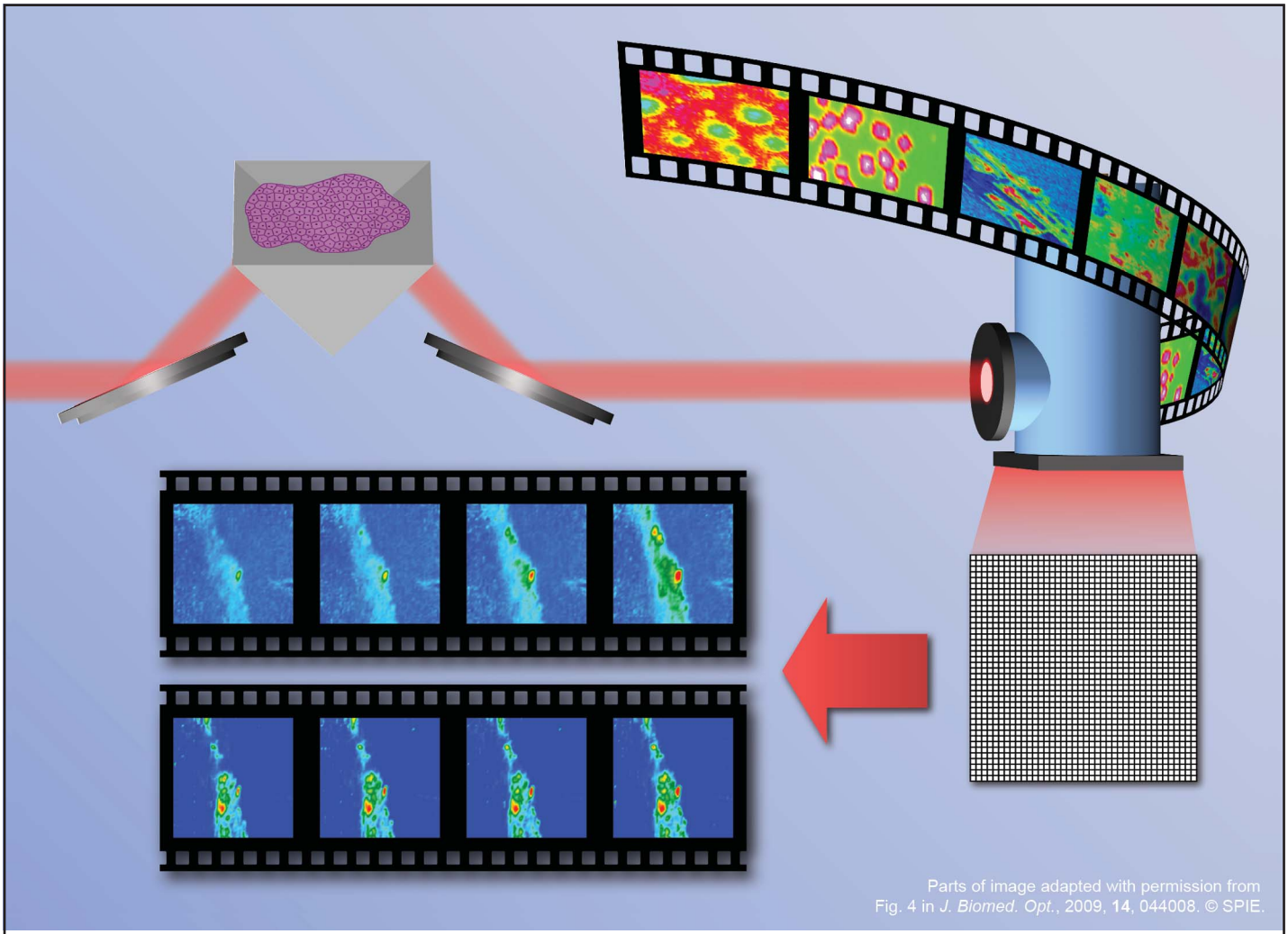

Parts of image adapted with permission from Fig. 4 in *J. Biomed. Opt.*, 2009, **14**, 044008. © SPIE.

Showcasing research of biological applications of spectroscopic imaging from the laboratory of Professor Sergei Kazarian at the Department of Chemical Engineering, Imperial College London, United Kingdom.

Title: ATR-FTIR spectroscopic imaging: recent advances and applications to biological systems

Infrared spectroscopic imaging is an emerging technology for studies of dynamic processes in biological samples such as aorta, skin and live cells, demonstrating its great potential for medical diagnosis and biomedical research.

As featured in:

See Sergei G. Kazarian and K. L. Andrew Chan, *Analyst*, 2013, **138**, 1940–1951.

RSC Publishing

www.rsc.org/analyst

Registered Charity Number 207890

Analyst

RSC Publishing

TUTORIAL REVIEW

ATR-FTIR spectroscopic imaging: recent advances and applications to biological systems

Cite this: *Analyst*, 2013, **138**, 1940

Sergei G. Kazarian* and K. L. Andrew Chan

Attenuated total reflection Fourier transform infrared (ATR-FTIR) spectroscopic imaging is a highly versatile, label free and non-destructive chemical imaging method which can be applied to study a wide range of samples and systems. This review summarises some of the recent advances and applications of this imaging method in the area of biomedical studies, including examples of section of aorta, skin tissue and live cells. Two of the major advantages of measuring in ATR mode are the opportunity to measure samples that absorb strongly in the IR spectrum, such as aqueous systems, without significant sample preparation and the ability to increase the spatial resolution of the measured image. The implications of these advantages as well as some limitations of this imaging approach are discussed and a brief outlook at some of the possible future developments in this area is provided.

Received 17th December 2012
Accepted 1st February 2013

DOI: 10.1039/c3an36865c

www.rsc.org/analyst

Introduction

FTIR spectroscopic imaging is a chemical imaging technique that can be applied to a broad range of samples and systems. The significant potential of this technique in the biomedical field is beginning to be realised with a number of new applications being introduced. One of the main advantages of FTIR imaging is that it is a fast and label-free imaging technology. As such, no dye or labelling methodology is needed. Therefore any possible interference from labelling species within the studied systems is eliminated and there is no need to develop, test or manufacture labelling chemistry. FTIR imaging provides a large number of spatially resolved infrared spectra, with high chemical specificity, arranged in an array format. The chemical specificity of FTIR imaging originates from the interaction (*via* absorption) of infrared light with the vibrational modes of the molecules being interrogated. The rich information contained in these FTIR spectra allows multiple chemical species to be tracked simultaneously and the representative images are generated from a single measurement. Image acquisition times can vary greatly depending on the approach employed to obtain

Department of Chemical Engineering, Imperial College London, SW7 2AZ, UK. E-mail: s.kazarian@imperial.ac.uk

Sergei G. Kazarian is Professor of Physical Chemistry in the Department of Chemical Engineering at Imperial College London. His research encompasses the fields of vibrational spectroscopy, supercritical fluids, intermolecular interactions and materials. In recent years his research has mainly been focused on the development and applications of spectroscopic imaging to materials, biomedical samples and pharmaceuticals. He has published over 170 articles and reviews in leading scientific journals and 11 book chapters. He was awarded an ERC advanced grant in 2008 for his work in spectroscopic imaging and presented his research at the Royal Society's 350th Anniversary Summer Science Exhibition in 2010.

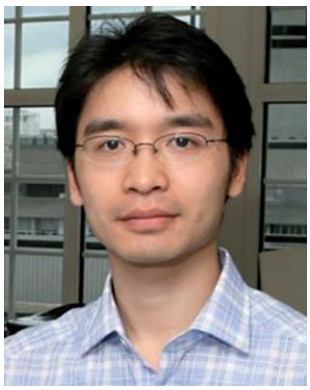

Andrew Chan obtained his PhD degree in 2004 (under the supervision of Prof. Sergei Kazarian) in Chemical Engineering from Imperial College London. He was then appointed as a post-doc before acquiring the EPSRC Life Science Interface fellowship in Prof. Kazarian's group, during which he had spent one year at Rutgers University in Prof. Rich Mendelsohn's laboratory as a visiting researcher. One of his main research interests is the development of new applications of spectroscopic imaging in pharmaceutical and biological systems. In September 2012, he was appointed as a lecturer in the Institute of Pharmaceutical Science at King's College London.

the array of spectral data. A few books and reviews on FTIR imaging in general have been published recently,[1–3] therefore the fundamentals of FTIR imaging will not be discussed in detail here. However, in brief, FTIR maps obtained by means of point by point mapping using an aperture in a microscope typically takes a few hours to complete. Fortunately, the use of array detectors (focal plane arrays (FPA) or linear arrays), which allow simultaneous detection of spatially resolved spectra, increase the acquisition speed by ~2 to 3 orders of magnitude. The development of FTIR imaging technology over the past 15 years has enabled high quality, diffraction limited FTIR imaging data to be collected in a few minutes to a few seconds.[4–8] Imaging has recently been demonstrated in the milliseconds time frame.[9,10] FTIR imaging has been useful in biomedical analysis such as for the study of biological tissues,[11–14] bone samples,[15] hair,[16,17] live cells,[18,19] diffusion of chemicals in skin,[20–22] skin wound healing[23] and dissolution of pharmaceutical formulations.[24,25] While this review will be focused on the application of ATR-FTIR to biomedical sciences in the past 5–6 years, reviews of specific applications of FTIR micro-spectroscopy to biomedical materials such as bone,[15] cells,[26] and biological tissues,[27] can be found elsewhere.

An FTIR image can be acquired mainly in three different configurations: transmission, reflection or attenuated total reflection (ATR). Depending on the nature of the sample, different modes of measurement are used. Transmission and transflection mode has been widely used for imaging biological tissues because tissue cross sections prepared for histological analysis can be readily used for FTIR imaging. However, rather than depositing the tissue cross sections on glass slides, the tissue samples are deposited on infrared transparent windows such as calcium fluoride or barium fluoride windows, or highly infrared reflective surfaces for transflection mode. These windows, while suitable as substrates for biological tissue, have a cut-off of light below ~1000 cm^{-1} and ~850 cm^{-1}, respectively, and are chosen such that the spectral region of interest is not affected by the transmission range of the substrate. Very recently, a "pseudo-hemisphere" CaF_2 lens, when applied to FTIR imaging in transmission mode, showed increased spatial resolution along with the removal of chromatic aberration and a reduction in scattering.[28]

Reflection mode is seldom used because samples are often not very reflective and polishing of biological material is not easy or desirable. ATR has been shown to be a highly versatile imaging mode[29] because the sampling path length does not depend on sample thickness and hence sample preparation is often not required. Furthermore, when an ATR objective is used in a microscope, the spatial resolution is enhanced due to the high refractive index of the ATR element. Indeed, images with spatial resolution well beyond the diffraction limit in air have been acquired.[30] In this article, we will only briefly describe the principle of ATR-FTIR imaging, a more detailed review on this technology can be found elsewhere.[31]

The principle of ATR-FTIR imaging

Conventional ATR-FTIR spectroscopy has been used for many years.[32] It is based on the attenuation effect of light when it is internally reflected at an interface between a high refractive index material (an internal reflection element) and an infrared absorbing low refractive index material (the sample). The light penetrates into the sample as an evanescent wave with the depth of penetration (the distance where the strength of the electric field decays to e^{-1}) shown in eqn (1).

$$d_p = \frac{\lambda}{2\pi n_1 \left(\sin^2 \theta - \left(\frac{n_2}{n_1} \right)^2 \right)^{0.5}} \quad (1)$$

Typical values of d_p for ATR-FTIR measurements range between 0.2 μm and 5 μm. It is important to note that the light penetrates into the sample beyond d_p and the information collected from the sample often goes up to 2 to 3 times the value of d_p.[33,34] A range of different accessories containing an internal reflection element can be used for ATR spectroscopy; such accessories may have a single or several internal reflections. The internal reflection element can be made of different infrared transparent materials and arranged in different configurations. However, in ATR-FTIR imaging only a single reflection can be used in order to retain integrity of the obtained image.

FTIR imaging in ATR mode is based on the combination of ATR-FTIR spectroscopy with imaging technologies. In conventional ATR-FTIR spectroscopy, a single element detector is used and a single spectrum is collected in each measurement. The spectrum collected then represents the average signal from the area of the sample that the light passed through. In ATR-FTIR imaging, a large number of spatially resolved ATR spectra are collected using an array detector. To date, there are mainly two types of mid-infrared array detectors that are commercially available, linear and focal plane array (FPA). A square 64 × 64 or 128 × 128 FPA allows the acquisition of thousands of spectra from a large sample area simultaneously. This combination of an FPA detector with micro ATR-FTIR imaging has been patented by Agilent.[35] We have quantitatively demonstrated that the imaging approach using array detectors effectively provide an enhancement in the sensitivity of ATR spectroscopy in a single measurement if an analyte is segregated in a localised area of the sample.[36] However, the spectral range of FPA detectors is restricted from the near-IR region to 900 cm^{-1} and the sensitivity of the measurement from individual pixels is generally poorer than those obtained with an ordinary single element detector. A 16 pixels linear array allows for the measurement of a larger spectral range (down to 720 cm^{-1}) with sensitivity similar to the ordinary single element mercury cadmium telluride (MCT) detector. However, images are generated from spectra obtained by rastering across the sample and the resulting images are therefore not collected simultaneously, limiting its application to static or very slow dynamic systems. These linear array and FPA detectors are combined with suitable optics such that an image can be collected. The magnification and spatial resolution of the resultant image depends on the type of optics employed. High magnification Ge micro ATR optics can produce high spatial resolution images but with small fields of view. Expanding optics, on the other hand, produce larger fields of view but low

Table 1 A summary of the imaging fields of view, spatial resolution and capabilities of various ATR imaging approaches currently available

	Imaging with FPA					Imaging with linear array
	Expanded field of view ATR	Variable angle ATR	Macro ATR	Diamond ATR	Micro ATR with Ge lens	Micro ATR with large Ge lens (~12 mm diameter)
Field of view/mm × mm	15.4 × 21.5	~3.9 × 5.5	2.6 × 3.6	~0.64 × 0.64	0.06 × 0.06	Up to 0.4 × 0.4
Spatial resolution (μm, estimated)	500	150	60	15–20	4	4–10
High-throughput applications (number of samples measured simultaneously)	Yes (>100)	Yes (100)	Yes (50)	Yes (<10)	No	No
Depth profiling	No	Yes	No	Yes	No	No

spatial resolutions. A summary of imaging field of view *versus* spatial resolution are shown in Table 1.

Properties of the ATR images

The small depth of penetration achieved through ATR implies that it measures a relatively thin layer of the sample that is in contact with the surface of an ATR element. Therefore, it is not just a surface technique. The same depth of penetration is applied to ATR imaging. A layer of the sample, a few micrometer thick, adjacent to the surface of the ATR crystal is probed by infrared light within the imaging field of view. The rest of the sample several micrometres beyond the surface will not be measured (unless the sample is microtomed, like for transmission measurements, that different layers are measured as a function of depth within the sample) and notably, it will not affect the measurement of the studied layer. This feature of ATR analysis allows samples to be measured directly without the need for prior cross sectioning, microtoming or polishing.

Simple sample preparation: *in situ* measurements

Significantly, the convenience of this type of measurement allows many different experiments to be performed *in situ*. For example, ATR-FTIR imaging has been applied to study the effect of surface properties on the crystallisation and adsorption of proteins from solution.[37–39] In these studies, protein solutions were directly deposited on the surface of the ATR element, which were modified by self-assembled monolayers to introduce different surface properties, and images were measured as a function of time. The protein crystals, which nucleated on the surface of the ATR element, were detected and distinguished from salt crystals without the need to remove the protein crystals.

In situ macro ATR-FTIR imaging has also been applied to study the diffusion of drug and macromolecules in atherosclerotic rabbit aorta[40] and drug diffusion in skin tissue.[20,41] In these cases the tissue samples were deposited on the ATR element and good contact was achieved without the need to apply any pressure. For dry tissues, a droplet of water could be added to slightly hydrate the tissue and improve contact between the tissue and the ATR crystal.[20] (A similar approach has also been used to improve the image quality of samples with greater hardness, such as cross-sections of paintings, where a droplet of water was used to fill the empty spaces that arose due to the surface roughness of the sample.[42]) The solution of drug was then added from the side of the sample which was followed by imaging the tissue as a function of time allowing the drug diffusion into tissue to be visualised. Macro ATR-FTIR imaging was used to study the diffusion of model drug molecules and macromolecules into and across samples of arterial wall.[40] The diffusion of two model drugs, benzyl nicotinate and ibuprofen, as well as the plasma macromolecule albumin, across atherosclerotic rabbit aorta was studied by *ex vivo* ATR-FTIR imaging. Benzyl nicotinate in Ringer's solution showed a higher affinity for atherosclerotic plaque than for apparently healthy tissue (see Fig. 1). The ability of albumin to act as a drug carrier for ibuprofen was demonstrated by multivariate image analysis.[40]

Another example of *in situ* measurements using both macro and micro ATR-FTIR imaging is the study of chemical changes in live cells.[43] The study of live cells with non-imaging ATR had shown some interesting developments.[44] Micro ATR-FTIR combined with imaging has demonstrated that it is possible to image live cells at a sub-cellular level.[43] Live cells were directly seeded and grown on the surface of a removable ATR crystal such that they formed good contact and were measurable in micro ATR mode. The schematic diagrams shown in Fig. 2a demonstrate how cells are seeded and maintained on the surface of an ATR element together with photographs (Fig. 2b) of the actual ATR plate. Spectra which can be used to elucidate the chemical composition inside live cells were extracted from different parts of the measured cells as also shown in Fig. 2c. The spectrum extracted from the nuclear region shows a stronger band at 1085 cm^{-1}, assigned to DNA phosphate backbone stretching vibrations, while the spectrum extracted from the cytoplasm region next to the nucleus shows a weaker band at 1085 cm^{-1}. Spatial variations of the absorbance of this band indicates the ability of micro ATR-FTIR imaging to probe chemical differences in live cells at sub-cellular resolution. In addition to biological tissue, macro ATR-FTIR imaging has also been applied to study bio-material processes including the coacervation of elastin under high-pressure CO_2.[45] The ATR surface was enclosed within a miniature high-pressure chamber where a small amount of the elastin solution was contained. It was then possible to expose the solution to various pressures of CO_2 and temperature while FTIR images were measured *in situ*.

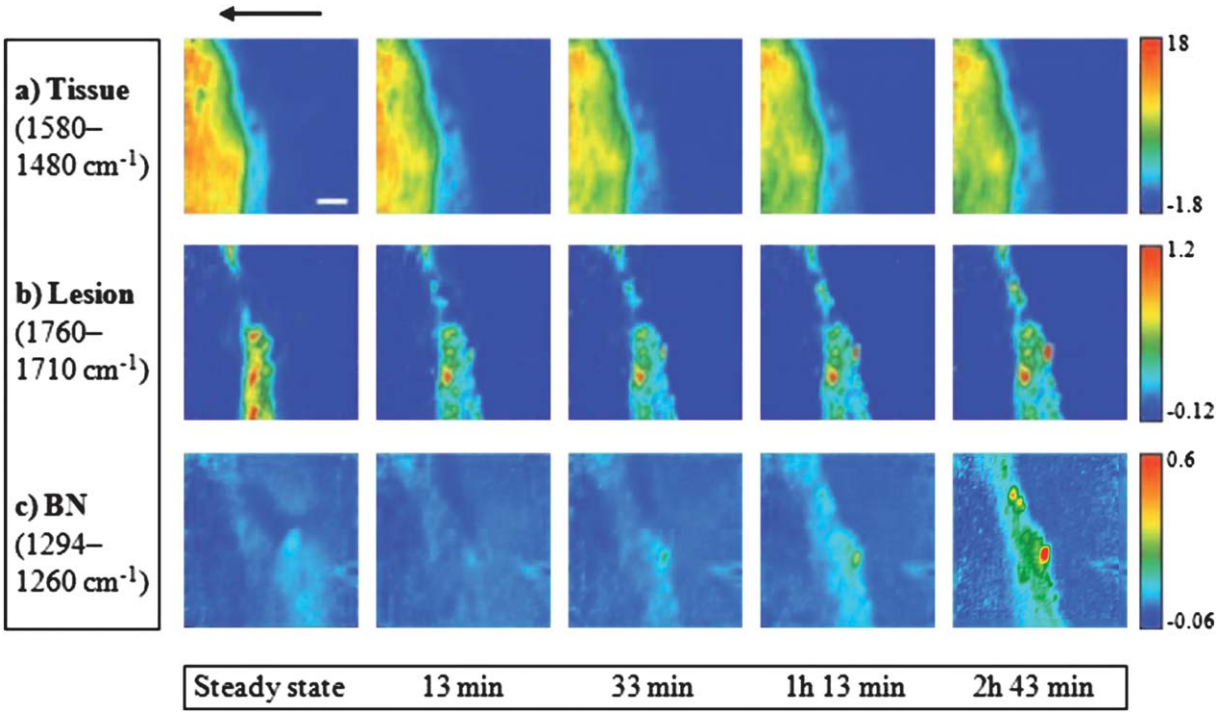

Fig. 1 Spectroscopic images of a diffusion experiment using benzyl nicotinate (BN)–saturated Ringer's solution and a longitudinal section of rabbit thoracic aorta with an atherosclerotic lesion. (a) ATR-FTIR images of the tissue downstream of the branch ostium obtained from the spatial distribution of the integrated absorbance of the amide II band, in the range 1580 to 1480 cm^{-1}. (b) A lesion is revealed by integration of the ν(C═O) ester band between 1760 and 1710 cm^{-1}. Scale bar: 100 μm. (c) ATR-FTIR images of the benzyl nicotinate distribution at this location of the tissue given by integrating the ν_{asym} (C═O) band, in the range 1294 to 1260 cm^{-1}. The arrow indicates the sense of the diffusion—from the endothelium to the interior of the aortic wall. (Reprinted with permission from F. Palombo, C. B. Danoux, P. D. Weinberg and S. G. Kazarian, *Measurement of drug and macromolecule diffusion across atherosclerotic rabbit aorta ex vivo by attenuated total reflection-Fourier transform infrared imaging*, *J. Biomed. Opt.*, 2009, **14**, 044008.)

It is also possible to perform *in vivo* studies for samples that are easily accessible, for example, for the measurement of the surface of skin, hair and nail areas that are of great interest both to the academic and industrial communities.

Small path length

All the experiments described previously involve the measurement of materials in contact (or submerged) in water which is very common for biomedical science studies. Traditionally, the measurement of IR spectra from aqueous samples was challenging due to the strong IR absorption of water. Despite the high water content in these samples, the full range of the IR spectrum (4000–900 cm^{-1}) remains accessible, including the ν(O–H) region. This is because of the small depth of penetration, which results in a small effective path length. Therefore samples that are investigated in the presence of strong infrared absorbers, such as the case with live cells in aqueous medium[43] or the formation of hydroxyl apatite from stem cells,[46,47] can be measured without saturation of the detector.

The small depth of penetration can be advantageous as discussed above. However, it is also important to understand the implications of this when applying ATR-FTIR imaging to study biomaterials. The small depth of penetration requires that samples are in intimate contact with the ATR element. The IR absorbance will decrease dramatically if there are any small gaps between the sample and the ATR element, even if the gap is only a fraction of a micrometer deep. Ekgasit *et al.* has shown, in a non-imaging ATR-FTIR measurement, that the presence of air gaps between the ATR element and the sample can be revealed by comparing the absorbance of the spectral band measured with two different polarisations of IR light.[48] It was found that soft tissues such as skin often self-adhered to the surface of the ATR element and the size of this gap, in such cases, is insignificant.[49] Since the attachment of the skin tissue to the ATR surface does not require pressing from the other side, imaging of the skin exposed in different controlled environments, such as humidity, can be made for studying skin hydration and dehydration *in situ* (see Fig. 3). It is essential to ensure that, when an absorbance distribution image is generated from measurements, the pattern of the distribution represents the real composition changes across the imaged area rather than being the result of variable optical contact across the imaged area.

Apart from optical contact, the small depth of penetration can create issues for some measurements even when the sample being measured is a liquid, and thus inherently forms a good contact with the surface of the ATR crystal. For example, recently, it has been demonstrated that ATR-FTIR imaging can be applied to image microfluidic systems,[50] which has been an important advance in bio-sciences.[51] However, when ATR-FTIR imaging was applied to measure water droplets flowing in

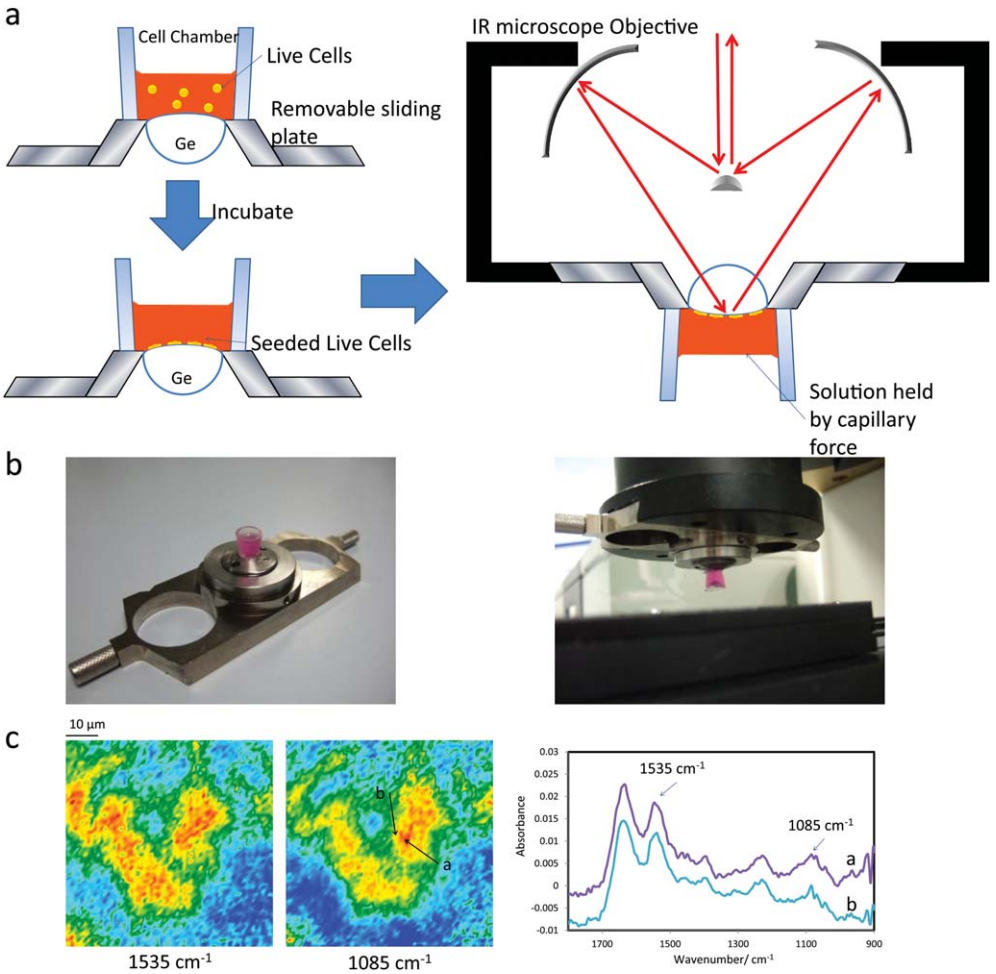

Fig. 2 (a) Schematic diagrams showing the procedure of seeding live cells on a removable ATR sliding plate (left) and how it is attached to the objective during measurement (right). (b) Photograph of the actual ATR sliding plate (left) and when it is integrated to the ATR objective (right). (c) FTIR images (left) generated using different spectral bands and the extracted spectra (right), after the subtraction of absorbance of water, from locations indicated on the FTIR image generated using the 1085 cm^{-1} band.

microfluidic devices,[52] the spectrum extracted from the water droplet region showed that the absorbance was dominated by the oil phase while the water spectral bands were barely detectable. The reason for this is that in the water-in-oil droplet, or segmented flow microfluidic system, the water droplets (or segments) were moving at a speed such that a thin layer of oil was formed between water droplets and the surface of the ATR crystal. As a result, the infrared light was mostly probing the oil layer and very little spectral information was collected from the water droplet region even though the oil layer was very thin (estimated to be ~0.8 μm). Another possible result due to the small depth of penetration is the "tip of the iceberg" effect where the apparent size of domains can be smaller than the actual size of the buried feature.[53] However, one could argue that the same limitation also applies to measurements in transmission or transflection mode where the sample often is a thin slice of the original sample.

Spatial resolution improvement

The diffraction limited image resolving power is given by the Rayleigh criterion in eqn (2).

$$r = \frac{0.61\lambda}{\mathrm{NA}} \quad (2)$$

where, NA is the numerical aperture of the system (the product of the refractive index, n, and sin θ and θ is half the angle of the collection of light, thus NA = n sin θ), λ is the wavelength of light and r is the minimal distance required to have a contrast of 26.4% between two nearby objects (just resolved). The objective in a typical infrared microscope usually offers a NA of ~0.4 to 0.6 such that r is approximately the same as the wavelength of light which is, for example, ~3 μm for ν(C–H), ν(O–H) and ν(N–H) bands, ~6 μm for carbonyl and amide I bands and ~10 μm for ν(C–C) and ν(C–O) bands. To completely resolve the features between the two objects without any significant spectral "contamination" due to diffraction, a minimum distance of 2r, which is the spatial resolution, is required. When imaging in ATR mode, IR light approaches the sample through a high refractive index material which provides an opportunity to increase the NA and thereby improve the spatial resolution. However, not all ATR imaging measurements would result in enhanced spatial resolution. For example, when ATR imaging is

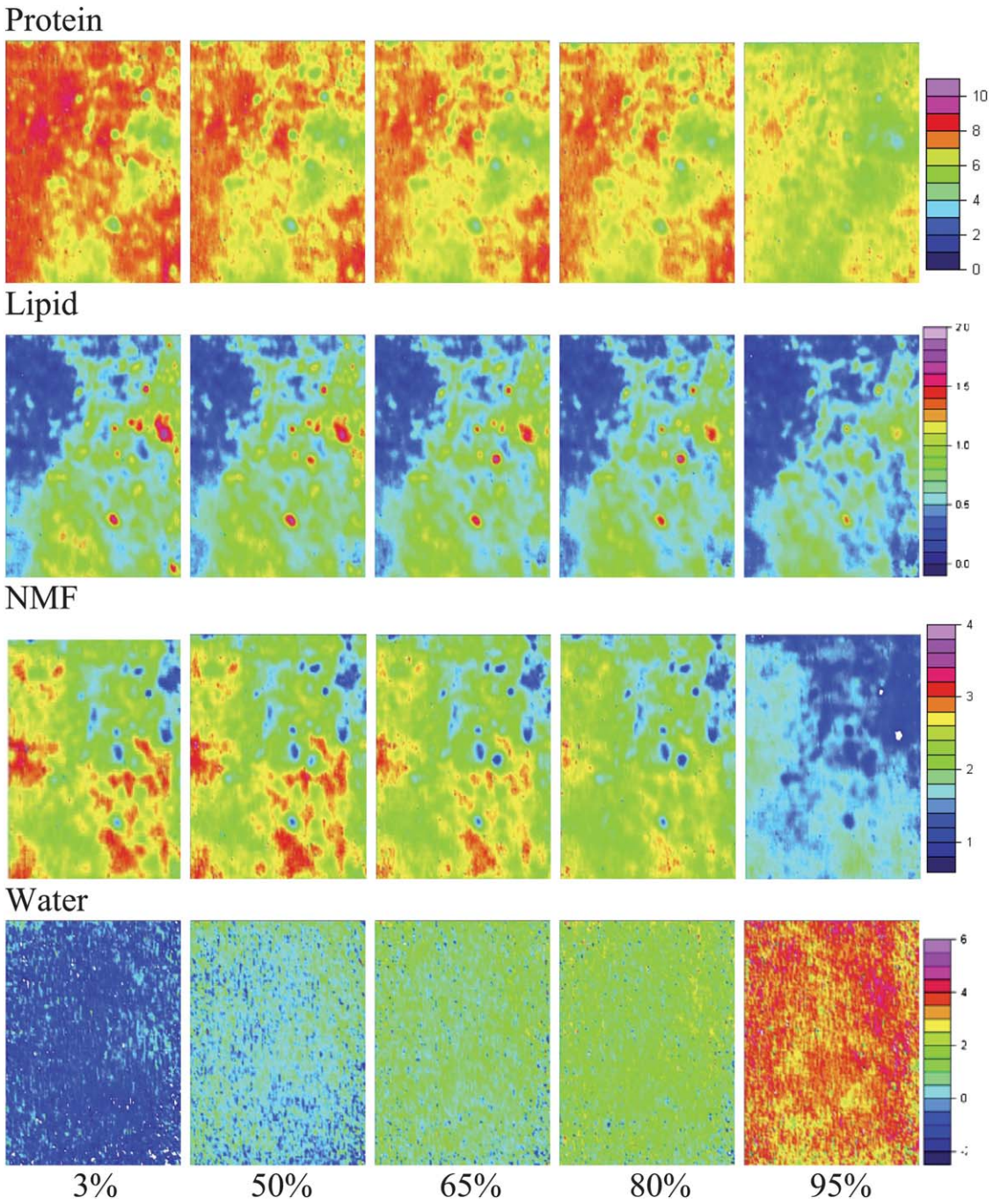

Fig. 3 Macro ATR-FTIR images of the *stratum corneum* at different controlled humidities. The images represent the distribution of different components, protein, lipids, natural moisturising factors (NMF) and water, which are labelled at the top of each row. The colour scale at each row has been adjusted to allow direct comparison to be made between images. The humidity levels are shown at the bottom of the images. The image size is approximately 900 μm × 1260 μm. (Reprinted with permission from K. L. A. Chan and S. G. Kazarian, *Chemical imaging of the stratum corneum under controlled humidity with the attenuated total reflection Fourier transform infrared spectroscopy method*, *J. Biomed. Opt.*, 2007, **12**, 044010. Copyright (2007) SPIE.)

measured through an inverted prism, the value of sin θ is reduced when light enters the prism through the flat surface as demonstrated in Fig. 4. The reduction in sin θ counters any gain in NA that was due to the higher refractive index of the ATR element and the resultant NA is approximately the same as the system without the prism. Spatial resolution would, however, be enhanced when the geometry of the ATR element resembles a hemisphere (see Fig. 4).

Most ATR measurements made in a microscope use a hemispherical shaped ATR element and hence an increase in spatial resolution with respect to measurements in transmission is observed. The spatial resolution can be increased up

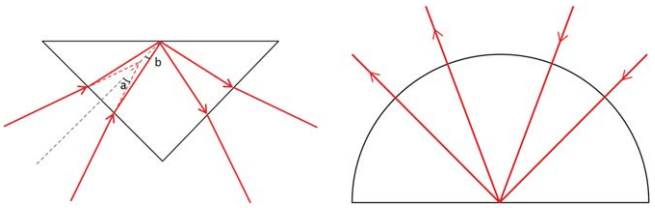

Fig. 4 Schematic diagrams showing the angle θ is reduced to b from a when image is made though an inverted prism (left) while the angle is not changed when imaging is made through a hemisphere (right).

to 4 times[30] with a Ge ATR element which has been employed to study live cells[43] where different cell organelles (nucleus and endoplasmic reticulum) were chemically imaged. Micro ATR imaging was also recently applied to study dried cells,[54] where changes in different subcellular compartments (cytoplasm and nucleus) were observed. The improvement in spatial resolution helped to detect small mineral inclusions of 2–3 μm in breast cancer tissue,[31] as well as distinguishing between endothelial cells, myoepithelial cells and terminal ductal lobular units in a breast tissue,[55] and preliminary imaging of chondrocytes in cartilage.[31,55,56]

In particular, the high spatial resolution of micro ATR-FTIR imaging proved to be very useful for the detection of microscopic components within plaques in arteries for understanding the progression of atherosclerosis.[11,57,58] For example, the results of our micro ATR-FTIR imaging study showed that dietary L-arginine supplements had beneficial effects in mature rabbit aorta, with an overall disappearance of the plaques.[58] The use of multivariate analysis when applied to the imaging data provided greater discrimination of different chemical species. The multivariate methods, such as principal component analysis and factor analysis were employed and relevant chemical and structural information were obtained. Two distinct protein constituents of the intima-media layer at different locations of the aorta wall were identified using the factor analysis method.[58] In collaboration with Cornell University,[11] micro ATR-FTIR spectroscopic imaging was applied *ex vivo* to the atherosclerotic aortic root of ApoE$^{-/-}$ and ApoE$^{-/-}$iNOS$^{-/-}$ mice fed with a high-fat Western diet. A reduction of lesion prevalence in ApoE$^{-/-}$iNOS$^{-/-}$ mice compared with ApoE$^{-/-}$ mice was detected. The analysis of the plaque region revealed spectral changes which may be indicative of protein nitration in the ApoE$^{-/-}$ mouse, which was a significant finding.[11]

Scattering reduction

Measurement of tissue in transmission mode or transflection mode FTIR often produces spectra with baseline effects as a result of resonant Mie scattering and/or specular reflectance, or the electric field standing wave effect.[59] It can then be necessary to apply a suitable correction algorithm to each spectrum.[60,61] The scattering effect is particularly strong near edges of tissues or when features with a high contrast in refractive index are approximately the same size as the wavelength of interrogating light. In ATR imaging, it has been shown that images and extracted spectra produce no observable scattering effects even when the sample contains small inclusions of mineral with a high refractive index.[13] Kidney tissue cross sections were imaged in transflection mode as well as in micro ATR mode. Apart from the improved spatial resolution observed in the images measured in micro ATR mode, the spectra extracted from the micro ATR measurements were free from sloping and derivative type baselines. This is in contrast to the spectra extracted from the same area of the sample measured in transflection mode, which shows strong sloping and derivative type baselines.

Variable depth of penetration

It is known that the depth of penetration of the IR light in ATR measurements, although small, can be manipulated to obtain extra depth information from a sample. According to eqn (1), the depth of penetration is a function of wavelength, refractive index of the ATR element and the angle of incidence. The angle of incidence is independent of the sample and can be changed with relative ease and therefore is often used as the parameter to adjust for depth profiling purposes. This property of ATR measurement is more often used in the analysis of polymer films or laminates[62] and recently has been shown to be applicable to biomedical imaging measurements.[34] The distribution of protein in *stratum corneum* tissue was found to be different when the angle of incidence was changed (a different depth of penetration was used).[34] Since depth profiling by changing the angle of incidence is not diffraction limited, it is possible to probe features in the nanometer scale in the "*z*-direction" as demonstrated in an ATR-FTIR imaging study on polymer films.[63]

However, when imaging in macro ATR mode, the depth of penetration dependence on the angle, beneficial for depth profiling studies, can result in an undesirable image artefact. Previous work[64] has shown that there was a spread of angles of incidence across the imaging area when using a particular ATR accessory. This led to an apparent concentration gradient of up to 16% across the imaged area even when the sample being imaged was a homogeneous liquid (Fig. 5). Such accessory was used to image rabbit aorta cross section with minimised baseline effect by self-modeling multivariate curve resolution methods.[65] However, the gradient effect as a result of the spread of angles of incidence would not be compensated by such mathematical means. We thought that this gradient effect was due to a lack of freedom of alignment (the mirrors are fixed) associated with that particular macro ATR accessory. As such, we carried out equivalent measurements using an alternative macro ATR accessory, where the mirrors can be aligned, showing no such gradient effect (Fig. 6).[66] It is therefore important to ensure that the alignment of the optics is optimised especially when quantitative analysis is carried out. The introduction of an aperture to reduce the diameter of the infrared light beam entering the macro ATR accessory may also be used to ensure that the spread of angles across the imaging area is insignificant.[67]

Contact pressure on biological tissues

While ATR-FTIR imaging has many advantages, the small depth of penetration requires physical contact between the ATR element and the sample. For samples that self-adhere to the

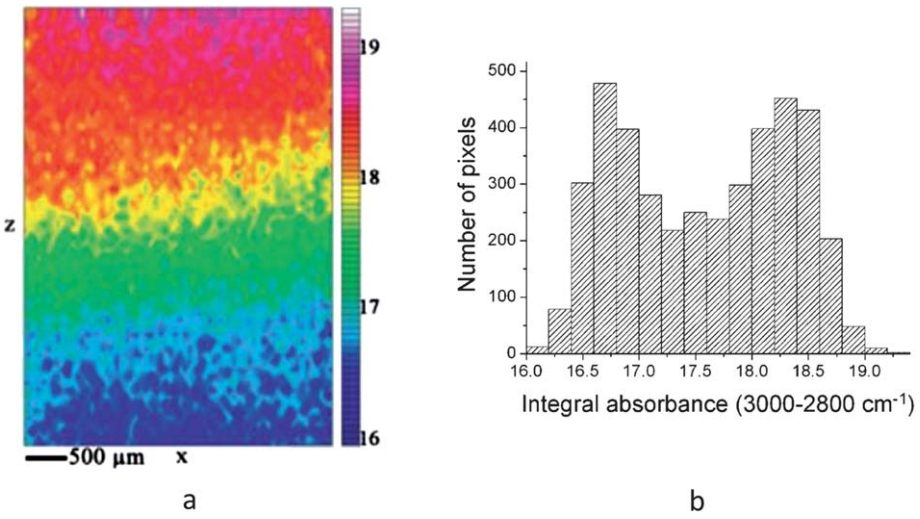

Fig. 5 ATR imaging results of paraffin oil for (a) $\nu(CH/CH_2/CH_3)$ absorption bands at 3000–2800 cm^{-1}. (b) Histograms: number of pixels *versus* integral absorbance of the ATR imaging measurements of paraffin oil for $\nu(CH/CH_2/CH_3)$ absorption bands at 3000–2800 cm^{-1}. (Reprinted with permission from E. Wessel, G. Heinsohn, H. Schmidt-Lewer-Kuehne, K. P. Wittern, C. Rapp and H. W. Siesler, *Observation of a penetration depth gradient in attenuated total reflection Fourier transform infrared spectroscopic imaging applications*, *Appl. Spectrosc.*, 2006, **60**, 1488–1492. Copyright (2006) Society of Applied Spectroscopy.)

ATR element with no pressure applied, it is not expected that contact results in tissue deformation. However, when tissue has already been mounted on a different substrate, for example a biopsy slide, some pressure will then need to be applied when the ATR element is brought into contact with the sample, which may result in deformation. The degree of possible deformation is related to the geometry of the ATR elements. For an inverted prism type ATR element such as those employed in macro ATR mode, the sampling surface is usually larger than or comparable to the size of the sample. In those situations, if pressure is needed to achieve contact, the sample will be compressed against a flat surface resulting in the uniform flattening of the sample. However, for samples measured in micro-ATR mode the contact area is usually considerably smaller than the size of the sample (except single cells)[68] and the micro-ATR element could possibly damage the soft biological tissue, leaving an indentation mark. Whilst the resultant ATR-FTIR measurement would capture an image of a flattened sample, the features may be slightly distorted and the same area of the tissue would not be suitable for re-analysis as the morphology may have been changed. Additionally, as demonstrated in the measurement of a single cell,[68] the smallest pressure on the cell can change the overall size of the cell by 18%. It is therefore important to always utilise the lowest amount of pressure required to capture an ATR-FTIR image to minimise the deformation or damage of tissue samples.[54,58]

Dispersion of refractive index

In ATR-FTIR measurements, depth of penetration, effective path length and hence the absorbance, is a function of

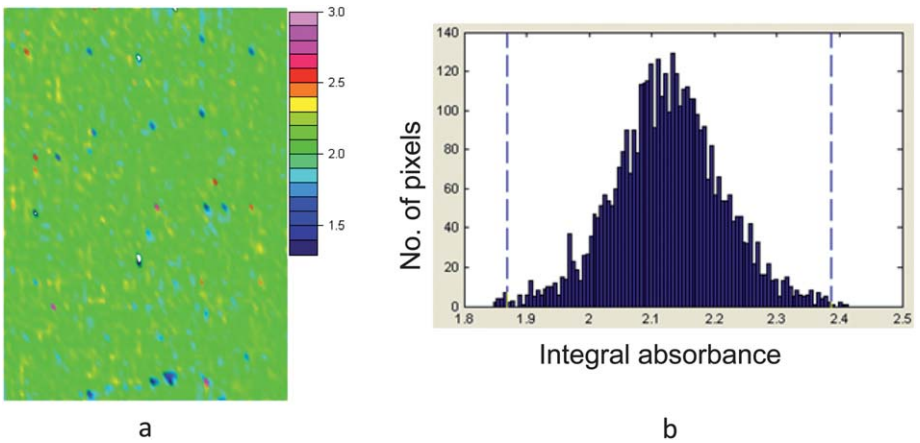

Fig. 6 ATR-FT-IR image of mineral oil measured with a ZnSe ATR accessory showing the integrated absorbance at 1480–1420 cm^{-1} in (a) 2D scale. (b) The histogram showing the number of detector pixels for different values of the integrated absorbance at the same range for the ATR-FT-IR measurement. (Reprinted with permission from S. G. Kazarian, K. L. A. Chan and F. H. Tay, in *Infrared and Raman Spectroscopic Imaging*, ed. R. Salzer and H. W. Siesler, Wiley-VCH, Weinheim, 2009, ch. 10, pp. 347–375. Copyright (2009) Wiley-VCH Verlag GmbH & Co. KGaA.)

wavelength and refractive indices of samples as can be noted from eqn (1). Dispersion of the refractive index of samples near the wavelength of an absorbance band may cause significant band shift. This is the known effect of anomalous dispersion[69] which can also produce a derivative-like baseline near spectral bands. The distortion of band shapes is often more pronounced when the ATR measurement is taken at an angle of incidence near the critical angle. A previous study on the measurement of samples with a high refractive index has shown that by increasing the angle of incidence, it is possible to reduce the distortion of spectral bands (Fig. 7).[70] Another study[71] on protein films using ATR-FTIR spectroscopy has shown that band shifts, as a result of anomalous dispersion, is more pronounced for stronger and wider bands. In that study, a shift in the amide I band was observed when the spectra were compared to those measured in transmission mode. However, the shift of the band was significantly reduced when a Ge ATR element was used instead of a diamond ATR element (Fig. 8).[71] It is therefore recommended that high refractive index ATR elements such as Ge and Si should be used, or increasing the angle of incidence when diamond ATR element is used,[31,67,70] for measuring high refractive index samples.

Outlook for the near future

ATR-FTIR imaging has been shown to be advantageous for its sample thickness independent measurement, ability to probe highly IR absorbing materials without significant sample preparations and the demonstrably improved spatial resolution as compared to other FTIR imaging approaches. Many of the recent advances in technology and applications have been discussed here. Nevertheless, there are still many new opportunities for further developments that are yet to be explored. One such possibility is the combination of ATR-FTIR imaging with a synchrotron source. ATR-FTIR imaging, due to the relatively small path length, often produces spectra with somewhat lower signal to noise ratio than spectra measured in transmission or transflection mode. FTIR spectra obtained from imaging experiments with the synchrotron source, on the other hand, provide an opportunity to produce spectra with high signal to noise ratios in a relatively short time frame.[72] Recently, a multi-beam synchrotron source has been employed to measure FTIR images in transmission mode with high spatial resolution and signal to noise spectra.[73,74] However, the combination of the synchrotron source with ATR-FTIR imaging is yet to be

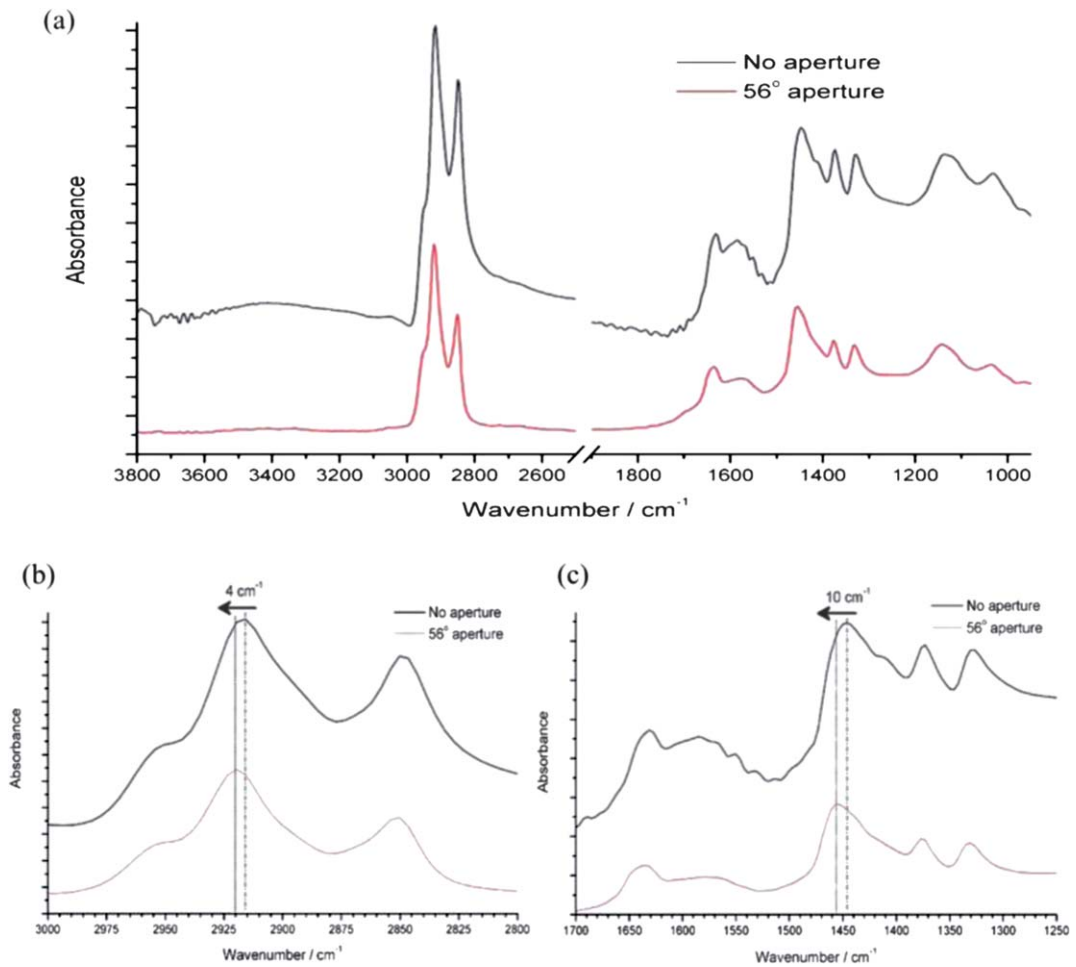

Fig. 7 (a) Single-element FTIR spectra of a sample with relatively high refractive index (deposit from crude oil) collected using a 47 and 56° aperture. Panels (b) and (c) show the distortions of the absorption bands at 3000–2800 cm^{-1} and 1700–1250 cm^{-1}, respectively. (Reprinted with permission from F. H. Tay and S. G. Kazarian, *Study of petroleum heat-exchanger deposits with ATR-FTIR spectroscopic imaging*, *Energy Fuels*, 2009, **23**, 4059–4067. Copyright (2009) American Chemical Society.)

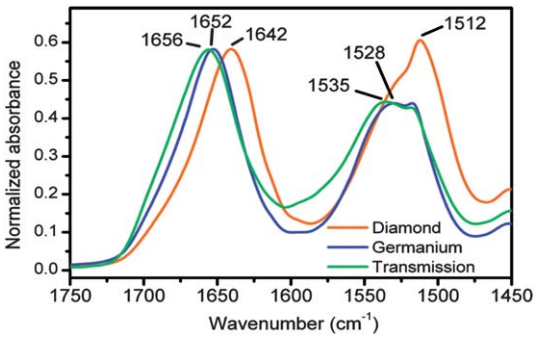

Fig. 8 Transmittance spectra and *s*-polarized diamond and germanium ATR spectra of a *B. mori* silk fibroin film. The spectra were normalized so that the peak heights of the amide I bands were equal. The germanium ATR spectrum has been multiplied by 5.98 with respect to diamond ATR. (Reprinted with permission from M. Boulet-Audet, T. Buffeteau, S. Boudreault, N. Daugey and M. Pezolet, *Quantitative determination of band distortions in diamond attenuated total reflectance infrared spectra*, *J. Phys. Chem. B*, 2010, **114**, 8255–8261. Copyright (2010) American Chemical Society.)

demonstrated. Other sources that can produce high brightness include the quantum cascade laser. These lasers are under rapid development and could become the next generation of IR sources that can bring the sensitivity level of FTIR measurements to a new level.[75]

As discussed earlier, ATR-FTIR imaging can be integrated with microfluidic devices for the chemical analysis of fluids flowing inside microfluidic channels (see Fig. 9).[50,76]

This idea can be expanded to the imaging, for example, of live cells cultured in microfluidic channels where the culture medium can be easily manipulated using the microfluidic technology while the chemical composition of the adhered live cells is monitored *in situ*. Although we have discussed that ATR imaging may not be well-suited to detect moving droplets, ATR-FTIR imaging can still be applied to study the droplets when they are stopped and allowed to make contact with the surfaces of the ATR element. Preliminary studies in our laboratory have shown that the water droplets flowing in oil start to have intimate contact with the ATR element surface when the flow has been stopped for approximately 1 s. This provides opportunities to design a microfluidic device that allows the water droplet to stop for a second or less within the imaged area for the analysis before continuing its journey in the microfluidic chip. The development of these approaches can be applied to cell analysis and cell sorting.[52] Forensic science may also benefit from the applications of the macro ATR-FTIR imaging, as it can produce chemical images of fingerprints collected with the aid of tape-lifting from different surfaces, thus providing chemical composition of a latent fingerprint which is a complex mixture of natural secretions of the body.[77]

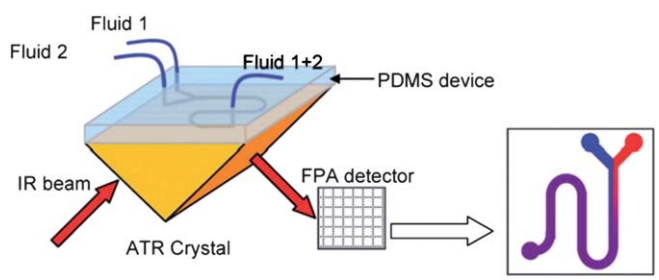

Fig. 9 Schematic diagram of ATR-FTIR imaging system and integration with a planar, chip-based microfluidic device. (Reproduced from ref. 50 with permission from The Royal Society of Chemistry.)

The enhanced spatial resolution of ATR-FTIR imaging clearly provides new insights into the analysis of cancer tissues for diagnostic purposes. Currently, the best demonstrated spatial resolution is on the order of a few micrometers. Improvements to spatial resolution would be an important development. Recently, a new technique that has been developed towards this goal is the combination of AFM with infrared spectroscopy that also uses an evanescent wave.[78] The idea is to detect the IR absorbance signal using an AFM cantilever based on the photothermal effect.[79] Since the detection mechanism is not photon based, image resolution is not diffraction limited. It has been demonstrated that it is possible to resolve 100 nm spatial features without labelling. However, at the moment, the speed of the measurement is relative slow compared to FTIR imaging, the spectral range is limited to 3600 cm^{-1} to 1200 cm^{-1} and the approach is only applicable to very thin samples. Nevertheless, as the technology matures in the next few years, it is anticipated the boundaries will be pushed forward. We contend that ATR-FTIR spectroscopic imaging, which is a truly emerging technology, will continue realising its great potential for biomedical research.

Acknowledgements

S. G. K. acknowledges research funding from the European Research Council under the European Community's Seventh Framework Programme (FP7/2007–2013)/ERC advanced grant agreement no. [227950].

References

1 R. Salzer and H. W. Siesler, *Infrared and Raman Spectroscopic Imaging*, Wiley-VCH Verlag GmbH & Co. KGaA, Weinheim, 2009.
2 G. Steiner and E. Koch, *Anal. Bioanal. Chem.*, 2009, **394**, 671–678.
3 S. Sasic and Y. Ozaki, *Raman, Infrared and Near-Infrared Chemical Imaging*, John Wiley & Sons, Inc., Hoboken, New Jersey, 2010.
4 J. L. Koenig and C. M. Snively, *Spectroscopy*, 1998, **13**, 22–28.
5 C. M. Snively, S. Katzenberger, G. Oskarsdottir and J. Lauterbach, *Opt. Lett.*, 1999, **24**, 1841–1843.
6 J. L. Koenig, *Adv. Mater.*, 2002, **14**, 457–460.
7 S. G. Kazarian and K. L. A. Chan, *Macromolecules*, 2003, **36**, 9866–9872.
8 A. Lanzarotta, L. Baumann, G. M. Story, M. R. Witkowski, F. Khan, A. Sommers and A. J. Sommer, *Appl. Spectrosc.*, 2009, **63**, 979–991.
9 K. L. A. Chan, X. Niu, A. J. deMello and S. G. Kazarian, *Anal. Chem.*, 2011, **83**, 3606–3609.

10 K. L. A. Chan and S. G. Kazarian, *Anal. Chem.*, 2012, **84**, 4052–4056.
11 F. Palombo, H. Shen, L. E. S. Benguigui, S. G. Kazarian and R. K. Upmacis, *Analyst*, 2009, **134**, 1107–1118.
12 R. Bhargava, *Anal. Bioanal. Chem.*, 2007, **389**, 1155–1169.
13 H. J. Gulley-Stahl, S. B. Bledsoe, A. P. Evan and A. J. Sommer, *Appl. Spectrosc.*, 2010, **64**, 15–22.
14 B. Bird, M. Miljkovic, N. Laver and M. Diem, *Technol. Cancer Res. Treat.*, 2011, **10**, 135–144.
15 A. Boskey and N. P. Camacho, *Biomaterials*, 2007, **28**, 2465–2478.
16 K. L. A. Chan, F. H. Tay, C. Taylor and S. G. Kazarian, *Appl. Spectrosc.*, 2008, **62**, 1041–1044.
17 G. J. Zhang, L. Senak and D. J. Moore, *J. Biomed. Opt.*, 2011, **16**, 7.
18 E. J. Marcsisin, C. M. Uttero, M. Miljkovic and M. Diem, *Analyst*, 2010, **135**, 3227–3232.
19 L. Chen, H. Y. N. Holman, Z. Hao, H. A. Bechtel, M. C. Martin, C. B. Wu and S. Chu, *Anal. Chem.*, 2012, **84**, 4118–4125.
20 J. M. Andanson, J. Hadgraft and S. G. Kazarian, *J. Biomed. Opt.*, 2009, **14**, 034011.
21 M. Boncheva, F. H. Tay and S. G. Kazarian, *J. Biomed. Opt.*, 2008, **13**, 064009.
22 J. Tetteh, K. T. Mader, J. M. Andanson, W. J. McAuley, M. E. Lane, J. Hadgraft, S. G. Kazarian and J. C. Mitchell, *Anal. Chim. Acta*, 2009, **642**, 246–256.
23 K. L. A. Chan, G. J. Zhang, M. Tomic-Canic, O. Stojadinovic, B. Lee, C. R. Flach and R. Mendelsohn, *J. Cell. Mol. Med.*, 2008, **12**, 2145–2154.
24 D. Velasco, C. B. Danoux, J. A. Redondo, C. Elvira, J. San Roman, P. S. Wray and S. G. Kazarian, *J. Controlled Release*, 2011, **149**, 140–145.
25 S. G. Kazarian and J. van der Weerd, *Pharm. Res.*, 2008, **25**, 853–860.
26 L. Quaroni and T. Zlateva, *Analyst*, 2011, **136**, 3219–3232.
27 G. Srinivasan and R. Bhargava, *Spectroscopy*, 2007, **22**, 30–43.
28 K. L. A. Chan and S. G. Kazarian, *Anal. Chem.*, 2013, **85**, 1029–1036.
29 S. G. Kazarian and K. L. A. Chan, *Biochim. Biophys. Acta, Biomembr.*, 2006, **1758**, 858–867.
30 K. L. A. Chan and S. G. Kazarian, *Appl. Spectrosc.*, 2003, **57**, 381–389.
31 S. G. Kazarian and K. L. A. Chan, *Appl. Spectrosc.*, 2010, **64**, 135A–152A.
32 N. J. Harrick, *Internal reflection spectroscopy*, John Wiley & Son, lnc, 1979.
33 F. M. Mirabella, *J. Polym. Sci., Polym. Phys. Ed.*, 1983, **21**, 2403–2417.
34 K. L. A. Chan and S. G. Kazarian, *Appl. Spectrosc.*, 2007, **61**, 48–54.
35 E. M. Burka and R. Curbelo, *US Pat.*, 6,141,100, 2000.
36 K. L. A. Chan and S. G. Kazarian, *Analyst*, 2006, **131**, 126–131.
37 S. Glassford, K. L. A. Chan, B. Byrne and S. G. Kazarian, *Langmuir*, 2012, **28**, 3174–3179.
38 K. L. A. Chan, L. Govada, R. M. Bill, N. E. Chayen and S. G. Kazarian, *Anal. Chem.*, 2009, **81**, 3769–3775.
39 S. E. Glassford, L. Govada, N. E. Chayen, B. Byrne and S. G. Kazarian, *Vib. Spectrosc.*, 2012, **63**, 492–498.
40 F. Palombo, C. B. Danoux, P. D. Weinberg and S. G. Kazarian, *J. Biomed. Opt.*, 2009, **14**, 044008.
41 J. M. Andanson, K. L. A. Chan and S. G. Kazarian, *Appl. Spectrosc.*, 2009, **63**, 512–517.
42 E. Joseph, C. Ricci, S. G. Kazarian, R. Mazzeo, S. Prati and M. Ioele, *Vib. Spectrosc.*, 2010, **53**, 274–278.
43 M. K. Kuimova, K. L. A. Chan and S. G. Kazarian, *Appl. Spectrosc.*, 2009, **63**, 164–171.
44 M. Schmidt, T. Wolfram, M. Rumpler, C. P. Tripp and M. Grunze, *Biointerphases*, 2007, **2**, 1–5.
45 F. Dehghani, N. Annabi, P. Valtchev, S. M. Mithieux, A. S. Weiss, S. G. Kazarian and F. H. Tay, *Biomacromolecules*, 2008, **9**, 1100–1105.
46 W. L. Randle, J. M. Cha, Y. S. Hwang, K. L. A. Chan, S. G. Kazarian, J. M. Polak and A. Mantalaris, *Tissue Eng.*, 2007, **13**, 2957–2970.
47 Y. S. Hwang, J. Cho, F. Tay, J. Y. Y. Heng, R. Ho, S. G. Kazarian, D. R. Williams, A. R. Boccaccini, J. M. Polak and A. Mantalaris, *Biomaterials*, 2009, **30**, 499–507.
48 S. Ekgasit and A. Padermshoke, *Appl. Spectrosc.*, 2001, **55**, 1352–1359.
49 K. L. A. Chan and S. G. Kazarian, *J. Biomed. Opt.*, 2007, **12**, 044010.
50 K. L. A. Chan, S. Gulati, J. B. Edel, A. J. de Mello and S. G. Kazarian, *Lab Chip*, 2009, **9**, 2909–2913.
51 A. Huebner, S. Sharma, M. Srisa-Art, F. Hollfelder, J. B. Edel and A. J. Demello, *Lab Chip*, 2008, **8**, 1244–1254.
52 K. L. A. Chan and S. G. Kazarian, *Spectroscopy*, 2012, **27**, 22–27.
53 N. J. Everall, I. M. Priestnall, F. Clarke, L. Jayes, G. Poulter, D. Coombs and M. W. George, *Appl. Spectrosc.*, 2009, **63**, 313–320.
54 S. E. Holton, M. J. Walsh and R. Bhargava, *Analyst*, 2011, **136**, 2953–2958.
55 M. J. Walsh, S. E. Holton, A. Kajdacsy-Balla and R. Bhargava, *Vib. Spectrosc.*, 2012, **60**, 23–28.
56 J. H. Yin and Y. Xia, *Biomed. Opt. Express*, 2011, **2**, 937–945.
57 C. S. Colley, S. G. Kazarian, P. D. Weinberg and M. J. Lever, *Biopolymers*, 2004, **74**, 328–335.
58 F. Palombo, S. G. Cremers, P. D. Weinberg and S. G. Kazarian, *J. R. Soc., Interface*, 2009, **6**, 669–680.
59 J. Filik, M. D. Frogley, J. K. Pijanka, K. Wehbe and G. Cinque, *Analyst*, 2012, **137**, 853–861.
60 P. Bassan, A. Kohler, H. Martens, J. Lee, H. J. Byrne, P. Dumas, E. Gazi, M. Brown, N. Clarke and P. Gardner, *Analyst*, 2010, **135**, 268–277.
61 B. Bird, M. Miljkovic and M. Diem, *J. Biophotonics*, 2010, **3**, 597–608.
62 L. J. Fina, *Appl. Spectrosc. Rev.*, 1994, **29**, 309–365.
63 T. Frosch, K. L. A. Chan, H. C. Wong, J. T. Cabral and S. G. Kazarian, *Langmuir*, 2010, **26**, 19027–19032.
64 E. Wessel, G. Heinsohn, H. Schmidt-Lewer-Kuehne, K. P. Wittern, C. Rapp and H. W. Siesler, *Appl. Spectrosc.*, 2006, **60**, 1488–1492.

65 D. S. Bu, S. W. Huffman, J. A. Seelenbinder and C. W. Brown, *Appl. Spectrosc.*, 2005, **59**, 575–583.
66 S. G. Kazarian, K. L. A. Chan and F. H. Tay, in *Infrared and Raman Spectroscopic Imaging*, ed. R. Salzer and H. W. Siesler, Wiley-VCH, Weinheim, 2009, ch. 10, pp. 347–375.
67 K. L. A. Chan, F. H. Tay, G. Poulter and S. G. Kazarian, *Appl. Spectrosc.*, 2008, **62**, 1102–1107.
68 T. P. Wrobel, K. M. Marzec, K. Majzner, K. Kochan, M. Bartus, S. Chlopicki and M. Baranska, *Analyst*, 2012, **137**, 4135–4139.
69 L. A. Averett, P. R. Griffiths and K. Hishikida, *Anal. Chem.*, 2008, **80**, 3045–3049.
70 F. H. Tay and S. G. Kazarian, *Energy Fuels*, 2009, **23**, 4059–4067.
71 M. Boulet-Audet, T. Buffeteau, S. Boudreault, N. Daugey and M. Pezolet, *J. Phys. Chem. B*, 2010, **114**, 8255–8261.
72 C. Petibois and B. Desbat, *Trends Biotechnol.*, 2010, **28**, 495–500.
73 M. J. Nasse, M. J. Walsh, E. C. Mattson, R. Reininger, A. Kajdacsy-Balla, V. Macias, R. Bhargava and C. J. Hirschmugl, *Nat. Methods*, 2011, **8**, 413–U458.
74 C. J. Hirschmugl and K. M. Gough, *Appl. Spectrosc.*, 2012, **66**, 475–491.
75 Y. Yao, A. J. Hoffman and C. F. Gmachl, *Nat. Photonics*, 2012, **6**, 432–439.
76 S. G. Kazarian, *Anal. Bioanal. Chem.*, 2007, **388**, 529–532.
77 C. Ricci, S. Bleay and S. G. Kazarian, *Anal. Chem.*, 2007, **79**, 5771–5776.
78 A. Dazzi, C. B. Prater, Q. C. Hu, D. B. Chase, J. F. Rabolt and C. Marcott, *Appl. Spectrosc.*, 2012, **66**, 1365–1384.
79 A. Dazzi, R. Prazeres, F. Glotin and J. M. Ortega, *Infrared Phys. Technol.*, 2006, **49**, 113–121.